A three-process-based distributed soil erosion model for catchment-scale on the Loess Plateau of China

Jingya Cai[a], Zuhao Zhou[a, *], Jiajia Liu[a], Hao Wang[a], Yangwen Jia[a], Chong-Yu Xu[b]

[a] State Key Laboratory of Simulation and Regulation of Water Cycle in River Basin, China Institute of Water Resources and Hydropower Research, Beijing 100038, China

[b] Department of geosciences hydrology, University of Oslo, Norway

Abstract

The Loess Plateau of China is one region in the world that suffers from the most severe soil erosion. In the gullied rolling loess region, approximately half of the sediment derives from gully areas, which are the most prominent topographical features of this region. No one of the existing soil erosion models stands out with advantages, such as accuracy or applicability, for the Loess Plateau because nearly all models only consider slope and river erosion processes at the catchment scale. The absence of the gully erosion process in these models significantly limits their application to the Loess Plateau. Taking this issue into account, a three-process-based distributed soil erosion model, WEP-SED, is proposed to investigate soil erosion in this region based on the Water and Energy transfer Processes in Large river basins (WEP-L) model. In

* Corresponding author. Tel.: +86 10 68785610. E-mail: zhzh@iwhr.com.

WEP-SED, a sequential “slope-gully-river” structure is built for the physically-based simulation of soil erosion and sediment yield. In this structure, soil erosion is integrated from six parts with successive transport relationships. The proposed model is applied to the upstream region of the Wenjiachuan hydrological station in the Kuye River basin. The simulated monthly average sediment transport rates from 1956 to 2010 at the Wenjiachuan hydrological station agree reasonably well with the observations, with a correlation coefficient of 0.76 and a relative error of -5.60%. Furthermore, the simulated average annual amount of gully erosion reaches 60.3% of the total soil erosion, reflecting the fact that the gully erosion is a serious problem and demonstrating that the gully erosion process must be considered separately in this area.

Keywords: gullied rolling loess region; physically-based; slope-gully-river; gully erosion; gravitational erosion

1. Introduction

Soil erosion is a geomorphic process in which soil particles, rock fragments, soil aggregates and organic matter are detached from their primary location and are transported to another (Poesen, 2018). The Loess Plateau in China is one region in the world that suffers from the most severe soil erosion (Xu, 1999; Zhang and Liu, 2005). The large crisscrossed and permanent gullies that fill in this region are unique features of the loess plateau, which contribute

significantly to the severe erosion (Jing, 1986; Tang and Chen, 1997). Erosion processes in a catchment that occur over slopes, gullies, and rivers are complicated. Previous studies have applied numerous soil erosion models to simulate soil erosion and sediment yield at the catchment scale on the Loess Plateau, such as the Watershed Erosion Prediction Project (WEPP) (Zhang et al., 2005; Li et al., 2011), Soil and Water Assessment Tool (SWAT) (Zuo et al., 2016), Morgan-Morgan-Finney model (MMF) (Li et al., 2010), and Digital Yellow River Model (DYRIM) (Wang et al., 2007). However, no model has stood out in terms of their accuracy or applicability (Li et al., 2017).

The commonly used soil erosion models can be categorized into three groups: empirical, conceptual and physically-based (Hajigholizadeh et al., 2018). Empirical models employ statistical techniques to reveal the relationships between the factors and components using only a linear regression or a relatively complex relationship, including multiple and nonlinear regressions (Wainwright and Mulligan, 2005). These empirical models, such as the Universal Soil Loss Equation (USLE) and Revised USLE (RUSLE), have simple computational processes and low data requirements (Wischmeier and Smith, 1978; Renard et al., 1997). These models may possibly perform well in one region but yield an insufficient performance in other regions because they are limited to certain conditions (Aksoy and Kavvas, 2005; Sadeghi et al., 2014). Conceptual models generally describe soil erosion and sediment transport processes without specific details (Hajigholizadeh et al., 2018; Merritt et al., 2003; Sorooshian, 1991).

Conceptual models, therefore, can indicate the effects of land use changes without requiring large amounts of spatially and temporally distributed input data. Conceptual models suffer from problems associated with the identifiability of their parameter values, which are obtained via calibration against observed data, such as flow discharge and sediment transport rates (Jakeman and Hornberger, 1993). The Erosion Productivity Index Calculator (original name) or Environmental Policy Integrated Climate (current name) (EPIC) (Williams et al., 1983) and Soil and Water Assessment Tool (SWAT) (Beven et al., 1989) are both typical conceptual erosion models. Physically-based models simulate the dynamic behavior of the concerned components in each soil erosion process generally based on the theoretical principles of kinematic wave procedures for routing sediment (Morgan and Quinton, 2001). The conservation equations of mass, momentum, and energy are fundamental for simulating soil detachment, sediment deposition, and sediment transport (Kandel et al., 2004). Recently, physically-based models including the Watershed Erosion Prediction Project (WEPP) (Laflen et al., 1991; NSERL, 1995), the Limburg Soil Erosion Model (LISEM) (De Roo et al., 1996), and the EUROpean Soil Erosion Model (EUROSEM) (Morgan et al., 1998) have been developed. These models are at the forefront of soil erosion research with several advantages, such as the incorporation of the underlying mechanisms of soil erosion and sediment transport (Pandey et al., 2016). There is, however, still a significant problem where most physically-based models are not sufficiently applicable to the Loess

Plateau because these models ignore the effects of gully erosion. These models usually only simulate two erosion processes, i.e. slope and river erosion, which do not conform to the fact that gully erosion has a significant contribution on the Loess Plateau (Jing, 1986). Because of the steep and unstable slopes with loose soil material in gully areas, the erosion mechanisms at these sites are different from river erosion (Hessel and Van Asch, 2003). The structure of these two-process models do not competently reflect and elucidate distinct topographical features with highly developed and heavily eroded gullies. Although gully erosion process has ever been considered in XIN-MIX-SED (Si et al., 2017) and DYRIM (Wang et al., 2007), the conceptual assumptions in XIN-MIX-SED, which is a lumped model, and the absence of scouring or deposition simulation in gullies in DYRIM both leave room for improving gully erosion simulations.

To simulate severe gully erosion, models must account for another issue, i.e., gravitational erosion, a critical factor that induces and contributes significantly to gully erosion on the Loess Plateau (Wang et al., 2007). The strong cohesion within dry loess gives gully banks extremely steep or even vertical slopes. When the moisture of loess increases (usually due to rainfall), cohesion will rapidly decrease as a power function of the moisture, leading to unstable banks and the easy collapse of large volumes of loess. Therefore, gravitational erosion is predominant in gully areas with sidewall gradients of

more than 25º and deeply cut gullies (Fu and Gulinck, 1994). There have been some achievements in research on the mechanism of gravitational erosion in gully areas (Wang et al., 2005), but these studies have infrequently implemented the gravitational erosion model at the catchment scale. In most previous soil erosion models, gravitational erosion is either usually ignored or estimated with an experimental formula (Cai et al., 1996).

Considering these issues, this paper proposes a physically-based distributed three-process soil erosion model, denoted by WEP-SED, to investigate soil erosion in gullied rolling loess regions of the Loess Plateau based on the existing Water and Energy transfer Processes in Large river basins (WEP-L) hydrological model. A three-level sequential "slope-gully-river" structure is built in WEP-SED to create a detailed simulation of soil erosion and sediment transport. The proposed model is applied to simulate soil erosion in the upstream region of the Wenjiachuan hydrological station in the Kuye River basin.

The rest of the paper is organized as follows. The soil erosion model and the WEP-L model are first introduced in Section 2. Then, the study area is described in Section 3. The simulation results are analyzed and discussed in Section 4. Finally, several conclusions are given in Section 5.

2. Materials and methods

2.1. Hydrological cycle simulation

The soil erosion model is based on hydrological process and, in this study,

we use the WEP-L model for river basins (Jia et al., 2006) to simulate the hydrological cycle. Previous studies have widely applied this model in different watersheds with various climate and geographic conditions (Jia and Tamai, 1998; Jia et al., 2004; Kim et al., 2005; Qiu et al., 2006). To obtain a WEP model that is applicable to water resource assessment in large basins, such as the Yellow River basin, several improvements are then made to establish the WEP-L model (Jia et al., 2006).

Fig. 1(a) shows the vertical structure of the WEP-L within a contour band while **Fig. 1(b)** shows the horizontal structure of the WEP-L within a watershed. In this model, land use is divided into five groups within a contour band, i.e., the Soil-Vegetation (SV), Non-irrigated Farmland (NF), Irrigated Farmland (IF), Water Body (WB), and Impervious Area (IA) groups. We simulate the horizontal processes in **Fig. 1(b)** for water transport using the hydrodynamic model with the following expressions:

$$\frac{\partial A}{\partial t} + \frac{\partial Q}{\partial x} = q_L, \tag{1}$$

$$S_f = S_0, \tag{2}$$

$$Q = \frac{A}{n} R^{2/3} S_f^{1/2}, \tag{3}$$

where t is simulation time (s), A is the water area perpendicular to the flow direction (m^2), x is the position along the flow direction (m), Q is discharge (m^3 s^{-1}), q_L is the lateral inflow along a gully or river per unit length (m^3 s^{-1} m^{-1}), S_f is the friction slope, S_0 is the river bed slope, n is the Manning coefficient, which

mainly depends on a river bed's surface roughness, and *R* is the hydraulic radius, which is a variable determined by the cross-sectional wetted area and perimeter (m).

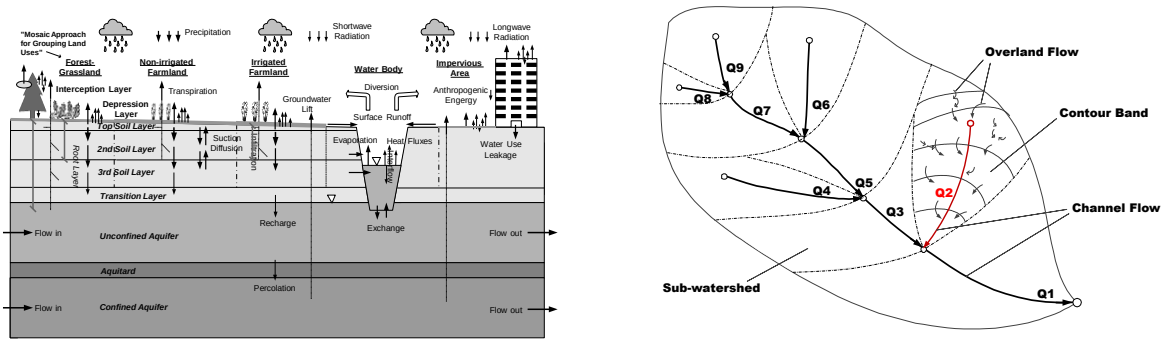

(a) **(b)**

Fig. 1. A schematic illustration of the WEP-L model structure: (a) the vertical structure within a contour band and (b) the horizontal structure within a watershed.

More details on WEP-L can be found in Jia et al. (2006). In this study, we propose a horizontal structure for the three-process water transport, i.e., the "slope-gully-river" (**Fig. 2**), which is an improved version of WEP-L, a two-process water transport mechanism, by including overland and channel flow. We separately take into account the gully process to reflect severe gully erosion on the Loess Plateau of China.

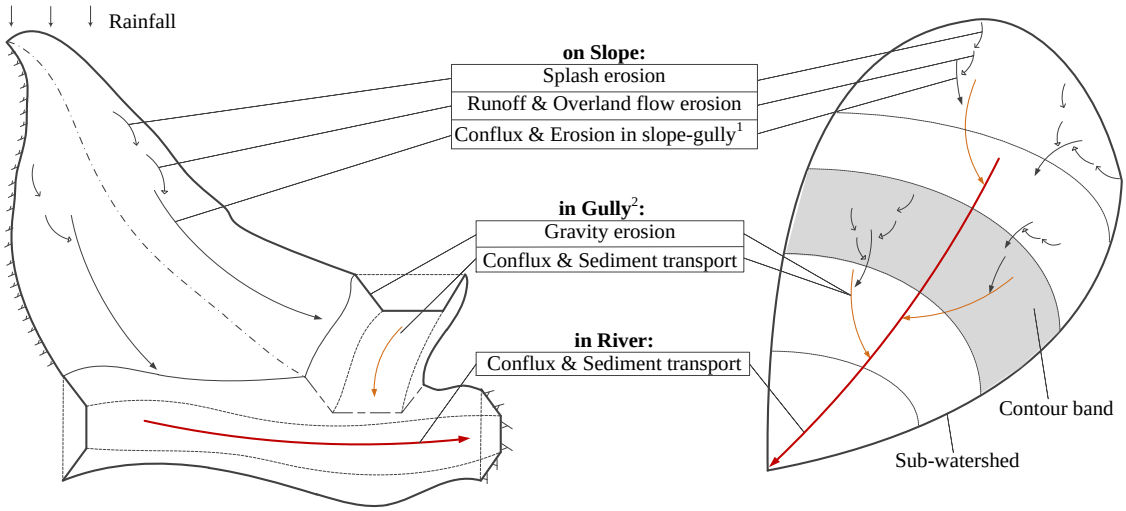

Fig. 2. A schematic illustration of the three-process hydrology and erosion simulation in the WEP-SED. 1: Slope-gully indicates gullies down-slope, such as rill and ephemeral gullies. 2: Gully indicates the gully at bottom of the slope, which is perpendicular to slope direction.

2.2. Soil erosion simulation

This study builds a three-process soil erosion model, i.e., the WEP-SED, to improve the WEP-L model by adding a new soil erosion and sediment transport module to it, enabling it to simulate soil and water loss on the Loess Plateau. Following the general physical process of soil erosion and sediment transport sequence in **Fig. 2**, **Fig. 3** shows a flowchart of the WEP-SED and all components included in this new model.

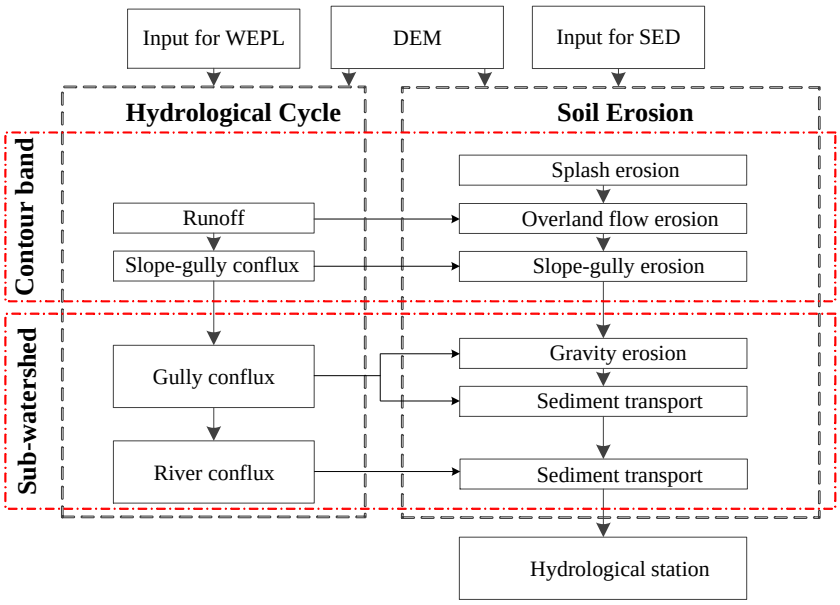

Fig. 3. A flowchart of the WEP-SED model.

2.2.1. Slope soil erosion

(1) Raindrop splash erosion

Hydraulic soil erosion generally begins with raindrop splashes. These can destroy soil texture and weaken the cohesive force of the inner soil, which detaches the original soil away from its source via overland flow. Splash erosion mainly occurs on bare land and is simulated based on the experimental results reported in Wu et al. (1992):

$$E_1 = a_1 \cdot (E_{rain} \cdot I_{rain})^{b_1} \cdot {\alpha_0}^{c_1} \quad (4)$$

where E_1 is the splash erosion intensity (kg m^{-2} s^{-1}), E_{rain} is the unit rainfall kinetic energy (J m^{-2} mm^{-1}), which was estimated from rainfall intensity on the Loess Plateau by Jiang et al. (1983), I_{rain} is the rainfall intensity (mm min^{-1}), α_0 is the representative slope angle gradient (°), and a_1, b_1, and c_1 are experimental coefficients.

(2) Overland flow erosion

Flow detaching effects on slope soil induce overland flow erosion. The detached soil can be estimated based on the flow discharge and slope gradient (He et al., 2003) with the following equation:

$$E_2 = a_2 \cdot q + b_2 \cdot q \cdot tan\alpha + c_2 \cdot tan\alpha + d_2 \quad (5)$$

where E_2 is the soil detachment rate (kg m^{-2} s^{-1}), q is the flow discharge per unit width (m^{-2} s^{-1}), and a_2, b_2,c_2, and d_2 are experimental coefficients.

The total soil loss on bare land, i.e., E_3, is constrained by the sediment flow transport capacity defined in Equation (6) (Prosser and Rustomji, 2000). The portion of soil that exceeds the sediment transport capacity is subtracted (deposited) from the soil detached via overland flow.

$$E_3 = \min\left(a_3 \cdot q^{b_3} \cdot (tan\alpha)^{c_3}/L_{Slo}, E_1 + E_2\right) \quad (6)$$

where E_3 is the total loss in soil intensity on bare land between a slope and gully (kg m^{-2} s^{-1}), L_{Slo} is the length of the contour band (m), and a_3, b_3, and c_3 are experimental coefficients.

Overland flow erosion mainly occurs on underlying surfaces, including forests, grasslands, bare, and slope croplands. Of these types of underlying surfaces, the erosion intensity and sediment transport on forests, grasslands, bare, and slope croplands can be determined with an adjustment coefficient in the following equation:

$$E_4 = E_3 \cdot (C_F \cdot F_F + C_G \cdot F_G + F_B + C_S \cdot F_S) \quad (7)$$

where E_4 is the comprehensive intensity of soil loss on bare land (kg m^{-2} s^{-1}); C_F,

210 C_G, and C_S are the adjustment coefficients for soil loss intensity in forests,
211 grasslands, and sloped croplands, respectively; and F_F, F_G, F_B, and F_S are the
212 percentage area of forests, grasslands, and sloped croplands, respectively, in the
213 current contour band.

214 **(3) Soil erosion in a slope-gully**

215 The amount of soil erosion in a slope-gully is determined by subtracting the
216 sediment eroded by raindrops and overland flow from the sediment flow
217 transport capacity in a slope-gully, as follows:

218 $$C_{SG} = \begin{cases} K_{SG} \cdot (T - C_4), & T > C_4 \\ 0, & T \le C_4 \end{cases} \quad (8)$$

219 where C_{SG}, T, and C_4 are the newly eroded sediment in a slope-gully (kg m^{-3}),
220 the sediment flow transport capacity in a slope-gully (kg m^{-3}), and the sediment
221 transported from splash and overland flow erosion (sediment from the adjacent
222 contour band above should also be added if the simulated contour band is not the
223 highest) (kg m^{-3}), respectively, and K_{SG} is the soil erosion coefficient in a
224 slope-gully.

225 Given the severe erosion that occurs in the study area, the sediment
226 transport capacity is determined with the equation derived by Zhang (1992) as
227 follows:

228 $$T = 2.5 \cdot \left[\frac{(0.0022 + C/\gamma_s) \cdot v^3}{\kappa \cdot \frac{\gamma_s - \gamma_m}{\gamma_m} \cdot g \cdot R \cdot \omega} \cdot ln\left(\frac{h}{6 \cdot d_{50}}\right)\right]^{0.62} \quad (9)$$

229 $$\kappa = \kappa_0 \cdot [1 - 4.2 \cdot \sqrt{C/\gamma_s} \cdot (0.365 - C/\gamma_s)] \quad (10)$$

$$\omega = \omega_0 \cdot \left(1 - \frac{\sqrt{C/\gamma_s}}{2.25 \cdot \sqrt{d_{50}}}\right)^{3.5} \cdot (1 - 1.25 \cdot \sqrt{C/\gamma_s}) \quad (11)$$

where κ and κ_0 are the Karman constants of muddy and clear water, respectively; γ_s and γ_m are the unit weights of dry soil and muddy flow, respectively (N m^{-3}); g is the gravitational acceleration (N kg^{-1}); R is the hydraulic radius (m); ω and ω_0 are the settling velocities of a sediment particle (m s^{-1}); C is the sediment concentration (kg cm^{-3}); v is the flow velocity (m s^{-1}); d_{50} is the median soil particle diameter, i.e., the ratio of soil particles smaller than a specific diameter of 50%; and h is the flow depth (m).

2.2.2. Gravitational Erosion

Among various types of gravitational erosion, collapses and landslides are the most dominant on the Loess Plateau (Cai et al., 1996). In this study, gravitational erosion mainly considers collapses simulated based on the mechanical equilibrium principle. The collapsed soil block can be generalized as a quadrangular prism unit, which has a trapezoidal transect (i.e., the profile of a collapsed soil block perpendicular to the direction of flow, similar to the bold polygon in **Fig. 4**).

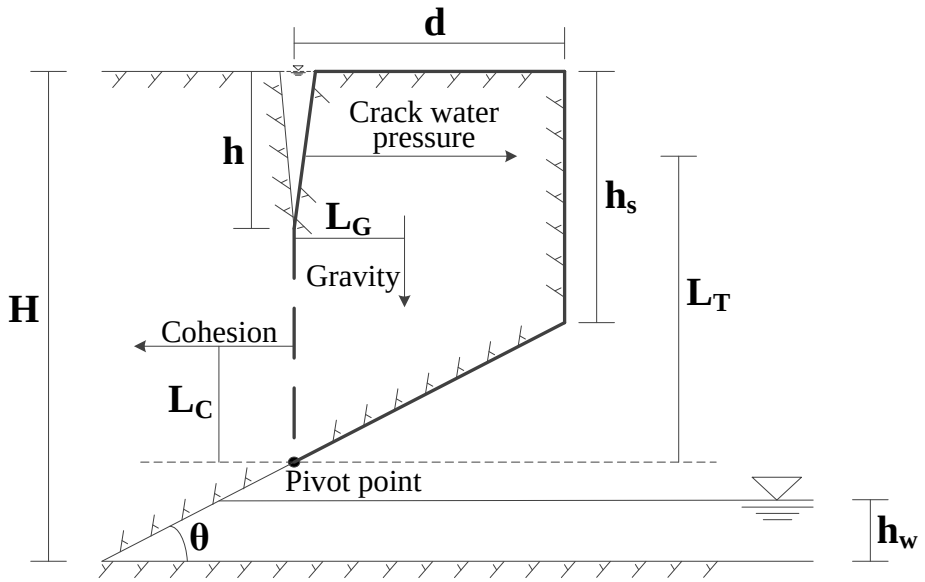

Fig. 4. A schematic of gravitational erosion.

The gravity of the collapsed soil block in **Fig. 4** can be estimated via geometrical analysis with the following equation:

$$M = \rho_m \cdot L \cdot (d \cdot h_s + 1/2 \cdot d^2 \cdot tan\ \theta) \quad (12)$$

where M is the mass of the collapsed soil block per unit length of gully per day (kg m^{-1} day^{-1}), ρ_m is the soil density (including the water contained in the soil) (N kg^{-1}), L is the average length of the collapsed soil block (along the flow direction) per meter of gully length (m), d is the thickness of the collapsed soil block (i.e., the height of the trapezoidal transect) (m), θ is the inclined angle between the scouring surface plane and horizontal plane, and h_s is the thickness of the outer edge of the collapsed soil block (i.e., the upper width of the trapezoidal transect) (m). For a collapsed soil block, we can use the torque equilibrium equation to calculate h_s.

The sidewall of the gully is usually stable because both gravity and cohesion affect the soil simultaneously. However, the cohesion of the inner loess

is sensitive to moisture; cohesion decreases rapidly with as moisture, such as rainfall, increases. At the same time, cracks appear in the soil that fill with rainfall and concurrently increase the water pressure on its soil block, resulting in the collapse of the sidewall. At this moment, there is a balance in the torque on the soil block, as shown in Equation (13), with which h_s can be calculated. Once the flow depth, h_w, in a gully reaches the soil block, the soil block will collapse as predicted in the torque-balanced situation (Equation (19)):

$$T \cdot L \cdot L_T + G \cdot L_G - c \cdot L \cdot 2L_C \cdot L_C = 0 \quad (13)$$

$$T = \frac{1}{2} \cdot \gamma \cdot h^2 \quad (14)$$

$$L_T = h_s + d \cdot tan\,\theta - h/2 \quad (15)$$

$$L_G = \frac{d \cdot (3 \cdot h_s + d \cdot tan\,\theta)}{3 \cdot (2 \cdot h_s + d \cdot tan\,\theta)} \quad (16)$$

$$c = 12000 + 462.27 \cdot w^{-2.5283} \quad (17)$$

$$L_C = (h_s + d \cdot tan\,\theta - h)/2 \quad (18)$$

$$h_w > H - (h_s + d \cdot tan\,\theta) \quad (19)$$

where T is the water pressure of the collapsed soil block per unit length (N m^{-1}), L_T is the force arm that corresponds to T (m), L_G is the force arm that corresponds to soil gravity, G (m), c is the cohesion forced on the soil block per unit area (N m^{-2}), w is the soil water content (%), L_C is the force arm that corresponds to c (m), h is the soil crack depth, h_w is the flow depth, and H is the gully depth.

2.2.3. Sediment transport in gullies and rivers

Sediment transport processes in both gullies and rivers are simulated based on the theory of non-equilibrium sediment transport. Considering sediment that is derived laterally from slopes along a gully or river, we can improve the non-equilibrium sediment transport equation as follows:

$$\frac{d(Q \cdot C_x)}{dx} = -\alpha \cdot B \cdot \omega \cdot (C_x - T_x) + Q_{ls} \quad (20)$$

where Q is the discharge in the channel ($m^3\ s^{-1}$) which is almost constant along a short channel; C_x is the sediment concentration at position x (kg m^{-3}); T_x is the sediment transport capacity at position x (kg m^{-3}); α is the saturation recovery coefficient, which generally vary from 0.021.78 with a mean value of 0.5; B is the channel width (m); L is the channel length (m); and Q_{ls} is the sediment transport rate that enters a unit length of channel laterally (kg s^{-1} m^{-1}).

Furthermore, we integrate equation (20), using the following equation to calculate that the subsequent at the gully and river estuary:

$$C_2 = T_2 + (C_1 - T_1) \cdot e^{-\frac{\alpha \cdot \omega \cdot L}{q}} + (T_1 - T_2 + \frac{Q_{ls}}{Q} \cdot L) \cdot \frac{q}{\alpha \cdot \omega \cdot L}(1 - e^{-\frac{\alpha \cdot \omega \cdot L}{q}}) \quad (21)$$

where C_2 and C_1 are the sediment concentration at the channel estuary and entrance, respectively (kg m^{-3}) (C_1 is 0 for the gully and upriver where there are no sub-watersheds; otherwise, sediment from all upper sub-watersheds should be added); and T_2 and T_1 are the sediment transport capacity at the channel estuary and entrance, respectively (kg m^{-3}). These variables are calculated with Equation (9) using the corresponding C_2 and C_1. The iterative method is necessary to calculate T_2 because the value of C_2 is unknown.

The lateral sediment sources, Q_{ls}, are different for a gully and for a river. In a gully, lateral sediment sources include portions of sediment from the slope-gully in the lowest contour band and portions from gravitational erosion. In a river, gully sediment is also a source of lateral sediment except for the portions of sediment that come from the slope-gully. Therefore, we calculate Q_{ls} for the gully, $Q_{ls,G}$, and river, $Q_{ls,R}$, with the following different equations:

$$Q_{ls,G} = p \cdot (E_{4,n} \cdot A_n + C_{SG,n} \cdot Q_{SG,n})/L_G + G/86400 \quad (22)$$

$$Q_{ls,R} = [(1-p) \cdot (E_{4,n} \cdot A_n + C_{SG,n} \cdot Q_{SG,n}) + C_G \cdot Q_G]/L_R \quad (23)$$

where p is the proportion of slope sediment that enters the gully, $E_{4,n}$ is the transported sediment from splash and overland flow erosion along the lowest contour band (kg m^{-2} s^{-1}), A_n is the area of the lowest contour band (m^2), $C_{SG,n}$ is the newly eroded sediment in the slope-gully along the lowest contour band (kg m^{-3}), $Q_{SG,n}$ is the discharge in the slope-gully along the lowest contour band (m^3 s^{-1}), L_G is the length of the gully (m), C_G is the sediment concentration in the gully of the currently simulated sub-basin (kg m^{-3}), Q_G is the discharge in the gully of the currently simulated sub-basin (m^3 s^{-1}), and L_R is the length of the river (m).

2.3. Assessment methods

To assess the agreement between the model simulations and observations, and to calibrate the model, we used three indicators: the correlation coefficient (R), the Nash–Sutcliffe Efficiency (NSE), and the Relative Error (RE) to

statistically analyze the model results.

R is used to assess the agreement between the observed and calculated monthly average discharge and sediment transport rates using the following equation:

$$\mathrm{R} = \frac{\sum_{t=1}^{T}(O_t-\bar{O})(M_t-\bar{M})}{\sqrt{\sum_{t=1}^{T}(O_t-\bar{O})^2}\sqrt{\sum_{t=1}^{T}(M_t-\bar{M})^2}} \quad (24)$$

where O_t is field observations; $\bar{O}$ is the average of O_t; M_t is the simulation; *t* is the time serial number; and *T* is the total number of observations. R ranges from 0 to 1 and values closer to 1.0 represent improved simulation results.

The NSE is also used to assess the agreement between the observed and calculated monthly average discharge and sediment transport rate. It uses the following equation (Nash and Sutcliffe, 1970):

$$\mathrm{NSE} = 1 - \frac{\sum_{t=1}^{T}(O_t-M_t)^2}{\sum_{t=1}^{T}(O_t-\bar{O})^2} \quad (25)$$

NSE ranges from –∞ to 1. Values of *NSE* between 0 and 1 indicate an acceptable level of performance, whereas values ≤ 0 indicate unacceptable performance since the mean observed value is a better predictor compared with the simulated value (Dutta and Sen, 2018).

RE is used in water and sediment balance analysis to assess overall model performance for the runoff volume and sediment yield. The RE is calculated with the following equation:

$$\mathrm{RE} = \frac{\sum_{t=1}^{T} O_t \cdot t - \sum_{t=1}^{T} M_t \cdot t}{\sum_{t=1}^{T} O_t \cdot t} \cdot 100\% \quad (26)$$

3. Study area and database

3.1. Kuye River Basin

The proposed model is applied to simulate soil erosion in the region upstream of the Wenjiachuan hydrological station in the Kuye river basin (**Fig. 5**), which has an area of 8,515 km^2. The basin is located in the eastern section of the transition zone between the Loess Plateau and the Mu Us Desert. There are occurrences of sparse vegetation, loose soil, broken terrain, and dense gullies in this area, with an average annual precipitation of 415 mm. The interannual variability in precipitation is high, with a maximum of 696 mm in 1964 and a minimum of 129 mm in 1965, i.e., only 20% of the maximum value. The seasonal precipitation distribution is also unevenly distributed, July and August storms account for 52% of the annual rainfall. Furthermore, a single storm may account for 10% of the annual rainfall (Hessel and Van Asch, 2003).

These geomorphological and climatic features render the study area one of the main sources of sediment in the Yellow River Basin. The average annual runoff measured at the Wenjiachuan hydrological station from 1953 to 2000 was 612 million m^3. The runoff in July and August accounted for 45% of the annual runoff, with uneven distribution spread throughout a year. The measured average annual sediment load is 100 million tons, which is more uneven than that of the runoff. The sediment load in July and August accounted for 90% of the annual total. The maximum historical sediment concentration at the Wenjiachuan

hydrological station is 1,700 kg m^{-3}, which is the maximum sediment concentration recorded for rivers globally (Xue and Lin, 2000). Therefore, this region has attracted significant attention for various hydrological studies.

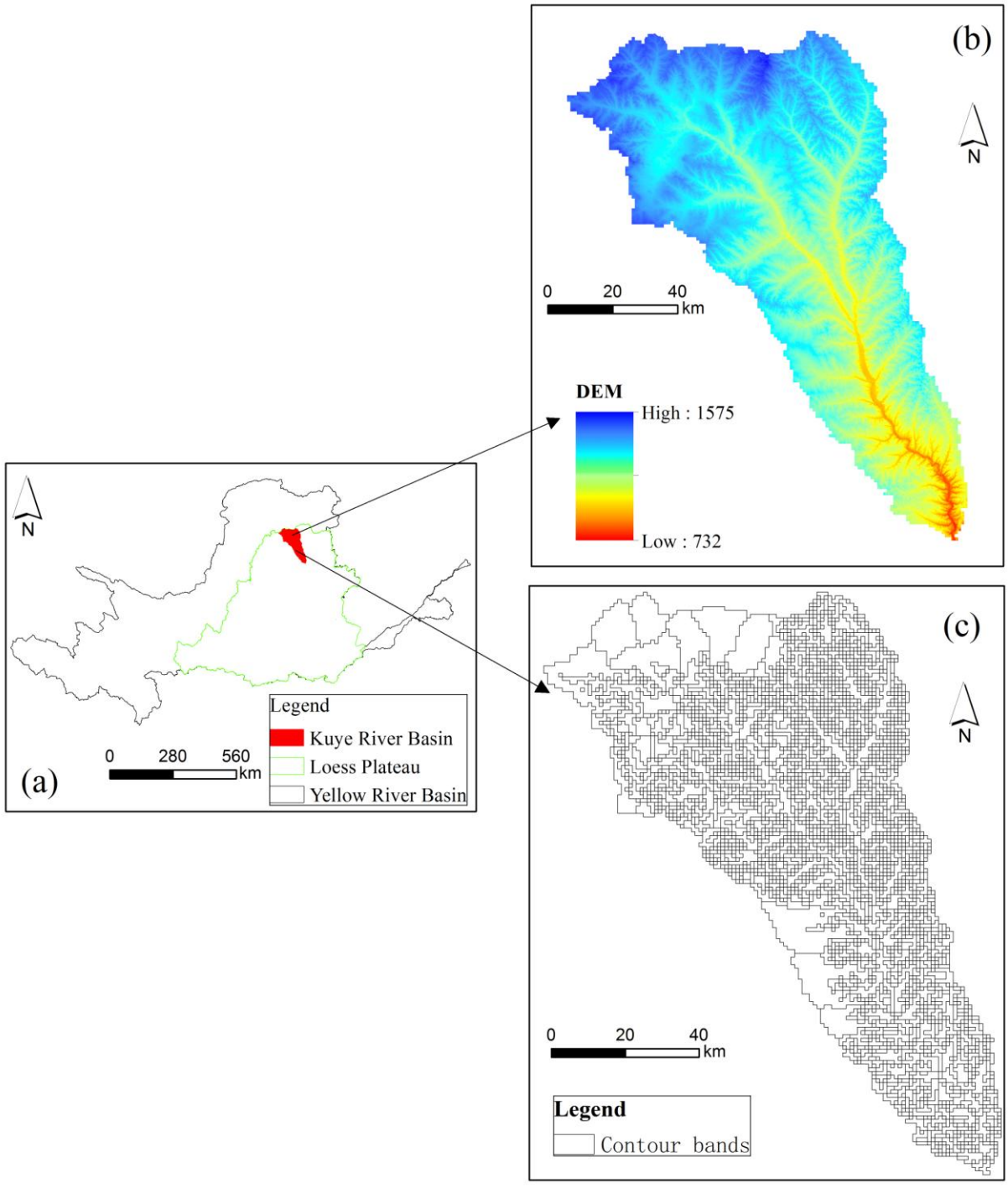

Fig. 5. The study area: (a) Location, (b) DEM, and (c) contour band division results.

3.2. Inputs and standard database

3.2.1. Model input data

Model input data mainly include hydro-meteorological data, underlying surface data (such as land use and soil and water conservation), topographic soil data (such as DEMs and soil types), and gully and river data (such as water system structures).

Hydro-meteorological data include daily rainfall, average temperature, sunshine, relative humidity, and wind speed at the main meteorological stations (there are 6 stations in the study area) from 1956 to 2010 provided by the China Meteorological Administration. For the underlying surface data, land use data were derived from Landsat TM data (1:1,000,000) for years 1980, 1985, and 1995 obtained from the Institute of Geographic Sciences and Natural Resources Research, Chinese Academy of Sciences. Land use before 1980 is identical to that of 1980. The linear interpolation method was used to calculate land use for other years. Soil and water conservation measures mainly include artificial forests, artificial grasslands, terraces, and check dams, obtained from China Water Statistical Yearbooks.

We used ASTER GDEM data (http://www.gscloud.cn/) with a spatial resolution of 30 m. Hydro-geological parameters, such as the hydraulic conductivity and specific yield, were provided by the Yellow River Conservancy Commission of the Ministry of Water Resources.

The actual water system, with a spatial resolution of 1:250,000 provided by the National Geomatics Center of China, is used to modify the DEMs to

improve the accuracy of the simulated river network. The gully and river sections are generalized into an inverted isosceles trapezoid. The upper bottom widths, lower bottom widths, and depths of the sections are required for the model and obtained by averaging the field measured values of several typical gullies and rivers.

3.2.2. Standard database

The available observational data for both monthly discharge and sediment transport rate at the Wenjiachuan hydrological gauge station cover 55 years, from 1956 to 2010, during which the observation series is completely continuous, as well as the model input database. These observational data were obtained from the Annual Hydrological Reports of the People's Republic of China.

4. Results

4.1. Model calibration and verification

4.1.1. Calibration results

Observations at the Wenjiachuan hydrological gauge station from 1956 to 1984 are used to calibrate the WEP-SED. **Figs. 6** and **7** show the observed and simulated monthly discharge and sediment transport rate during the calibration period.

411

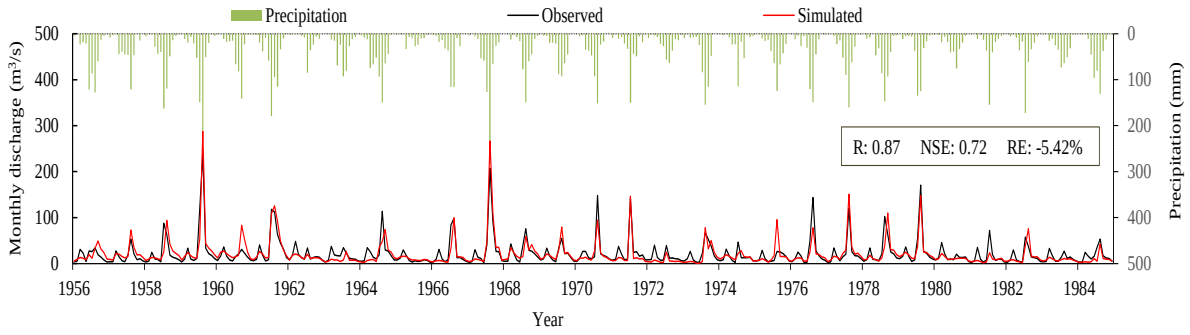

412 **Fig. 6.** The observed and simulated monthly discharge during the calibration period at the

413 Wenjiachuan hydrological station.

414

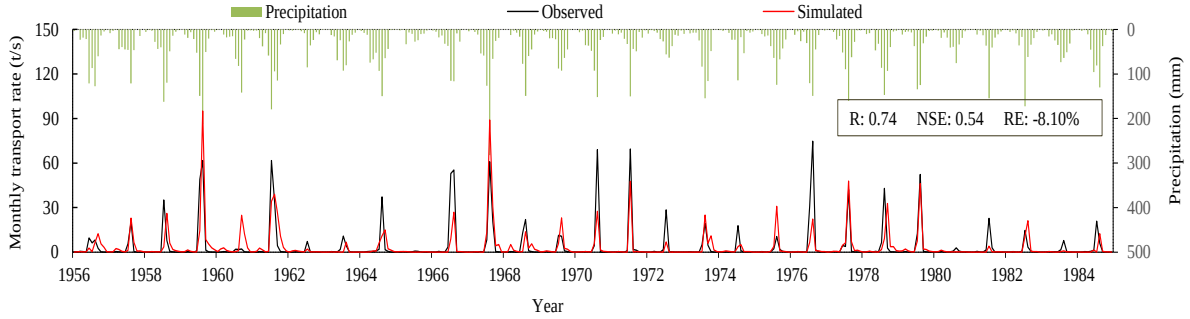

415 **Fig. 7.** The observed and simulated monthly sediment transport rate during the calibration

416 period at the Wenjiachuan hydrological station.

417 **Figs. 6** and **7** show that the simulations are consistent with the observations,
418 especially for peak values. The NSE is larger than 0.50 and the absolute relative
419 error is smaller than 10.0.0% both for discharge and sediment transport rate. All
420 three statistical indicators showed in **Figs. 6** and **7** demonstrate acceptable model
421 performance. Compared with the observations, the error between the simulations
422 and observations in **Fig. 7** is similar to the error in **Fig. 6**. It reflects that a large
423 error between the simulated and observed sediment transport rate corresponds to
424 a large error in the discharge simulation, which indicates that the soil erosion
425 model is significantly affected by the hydrological model.

426 **4.1.2. Verification results**

After model parameter calibration, the observations from 1985–2010 are used for model verification. **Figs. 8** and **9** show the observed and simulated monthly discharge and sediment transport rate during the verification period.

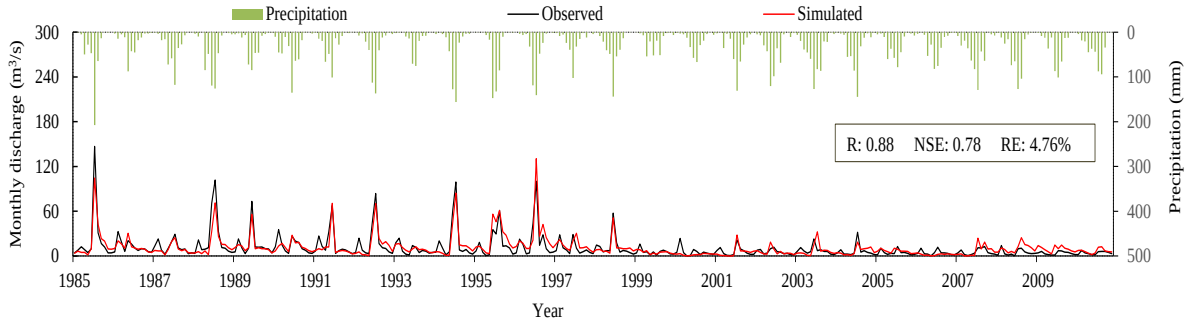

Fig. 8. The observed and simulated monthly discharge during the verification period at the Wenjiachuan hydrological station.

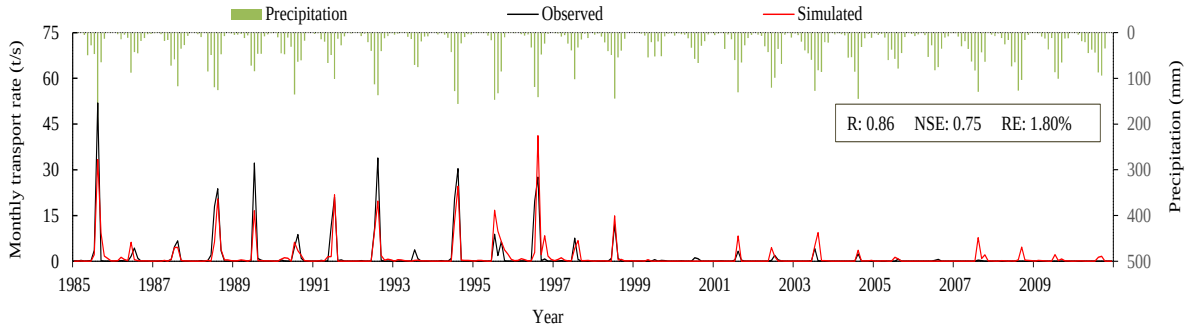

Fig. 9. The observed and simulated monthly sediment transport rate during the verification period at the Wenjiachuan hydrological station.

The calibrated WEP-SED performs well during the verification period as the NSE is larger than 0.75 and relative error is smaller than 5.0%. The three indicators are much better than those in the calibration period for sediment simulation. This better performance surely verifies the model calibration.

4.2. Gully erosion results

Gully erosion is an important and independent process of soil erosion on the Loess Plateau. Gully erosion occupies a large part of total soil erosion, larger

than both slope and river erosion. To investigate the contribution of gully erosion further, **Fig. 10** shows annual gully erosion and its ratio of contribution to the total erosion from 1956 to 2010.

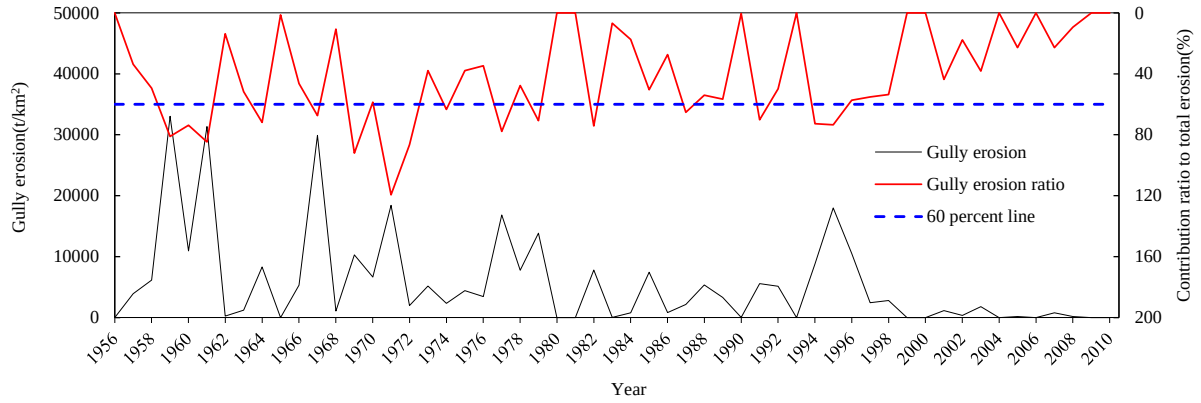

Fig. 10. The annual gully erosion from 1956 to 2010 in the Kuye River basin upstream of the Wenjiachuan hydrological station.

The average contribution of gully erosion to the total erosion is 60.3% from 1956 to 2010. This result is similar to the statistics showing that 60–70% of the sediment derives from gully erosion in the gullied rolling loess region (Fang et al., 1998).

Because heavy storm always occurs in several months from July to September, gully erosion appears to have significant variation throughout a year, as shown in **Figs. 11** and **12**.

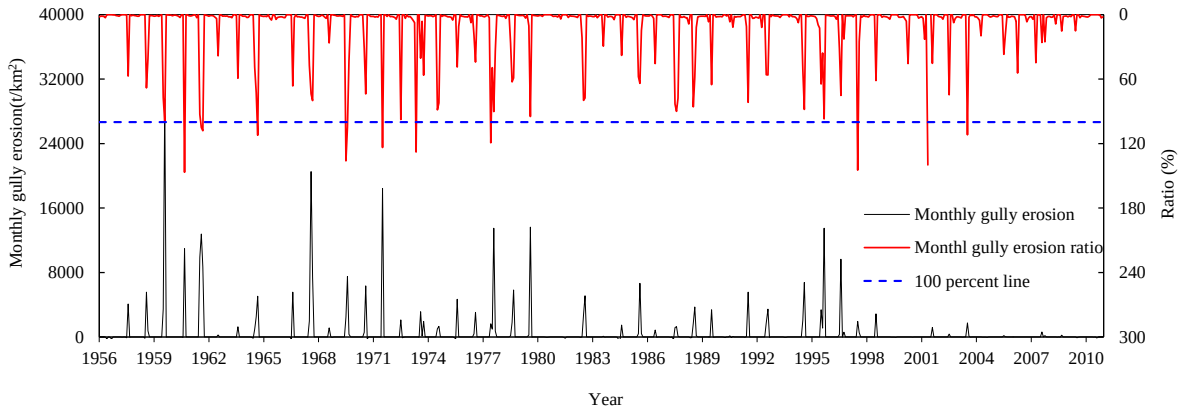

456

457 **Fig. 11.** Monthly gully erosion from 1956 to 2010 in the Kuye River basin upstream of the

458 Wenjiachuan hydrological station.

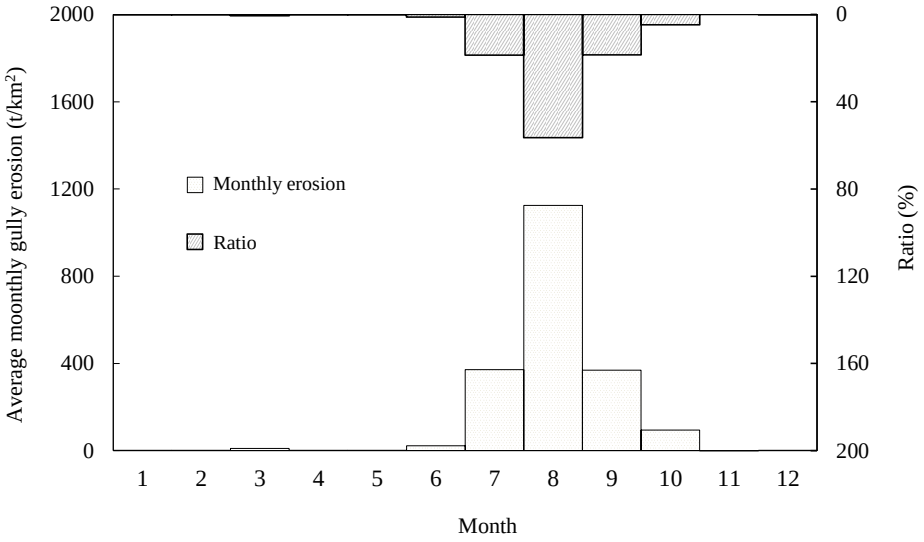

459

460 **Fig. 12.** Average monthly gully erosion from 1956 to 2010 in the Wuding River basin upstream

461 of the Wenjiachuan hydrological station.

462 Both the amount and contribution of gully erosion vary from month to

463 month, and nearly all the gully erosion occurs during June to October. In

464 particular, there are 13 months having a contribution ratio larger than 100%,

465 representing an extreme situation in which severe erosion occurs in gullies and

466 deposition occurs in rivers. The results of gully erosion can be seen from 1956 to

467 2010 in **Figs. 10** to **12**, which provide a strong evidence that gully erosion must

be considered separately from river process to better simulate soil erosion in this area, especially for the rainy seasons.

4.3. Gravitational erosion analysis

As previously mentioned, gravitational erosion is an important process during soil erosion, and improvements to simulate gravitational erosion also contribute significantly to improve WEP-SED performance compared with previous soil erosion models.

Fig. 13 shows that gravitational erosion contributes 7.93% of the total soil erosion. In particular, the contribution ratio of gravitational erosion to total erosion is even larger than 100% for several years, indicating that sediment derived from gravitational erosion is not completely transported out of the catchment but deposited in gullies or rivers. Considering recorded gravitational erosion in the Liudaogou, Chabagou, and Wuding River basins near the Kuye River basin, this result, i.e., a contribution ratio of approximately 10.0% for the gravitational erosion at Wenjiachuan is reliable (Guo, 2018). These results remind us again that gully erosions and gravitational erosion in gully areas, should be considered separately.

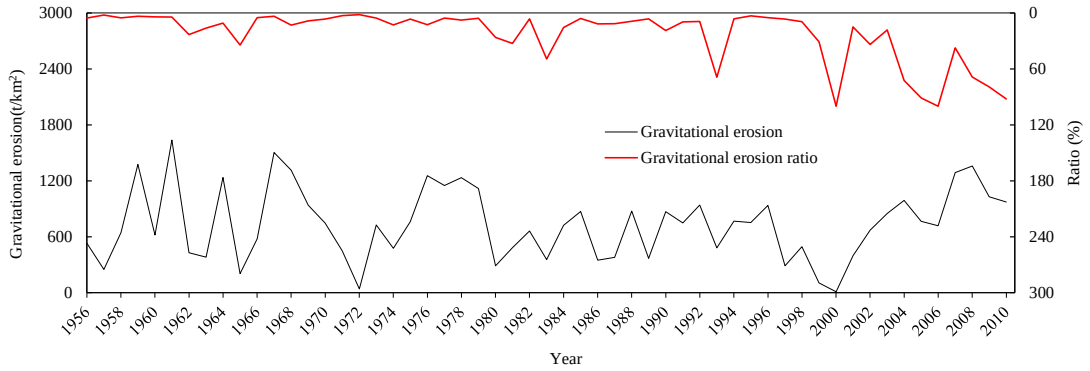

Fig. 13. Average annual gravitational erosion from 1956 to 2010 in the Kuye River basin upstream of the Wenjiachuan hydrological station.

5. Discussion

5.1. Model performance assessment

A complete model assessment is then performed for the entire period covering the 55 years and the results are listed in **Table 1** and shown in **Fig. 14**. Both simulated runoff and sediment yield are smaller than observed, as nearly all the relative errors are negative. The linear fitted relationship between simulated and observed monthly discharge is closer to the 1:1 line in **Fig. 14(a)**. All three indicators for the simulated discharge perform better than those of the simulated sediment transport rate as expected. However, the three indicators for simulated sediment transport rate reach a pretty high performance when compared to previous research results for the Loess Plateau, where a NSE less than 0.50 and a relative error larger than 20% (Li et al., 2017). The long simulation period and daily timescale further demonstrate the feasibility and efficiency of WEP-SED to simulate soil erosion. The simulation results of the WEP-SED model are reliable for further analyses related to soil erosion on the

503 Loess Plateau.

504

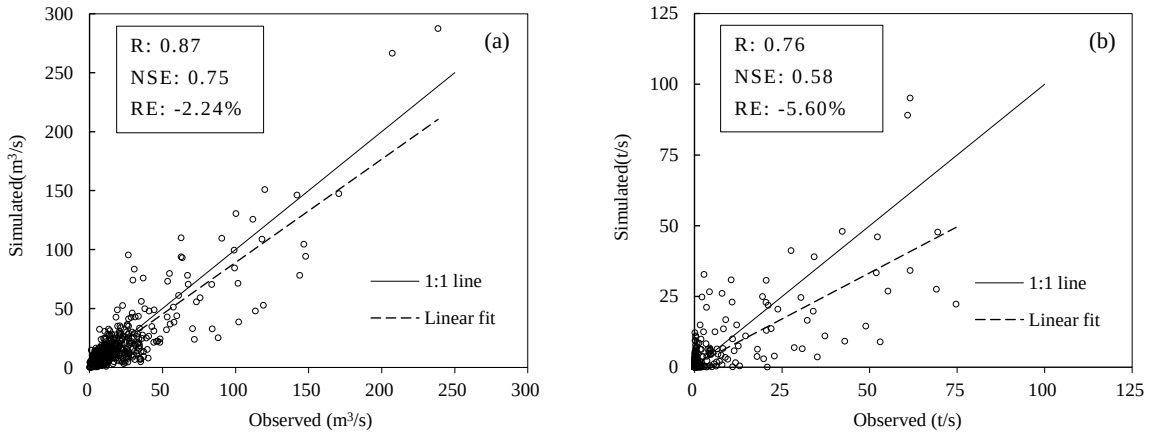

505 **Fig. 14.** Monthly discharge (a) and sediment transport rate (b) at the Wenjiachuan hydrological
506 station from 1956 to 2010.

507 However, there are several differences between the simulations and
508 observations that cannot be ignored. In both **Figs. 7** and **9**, the large peak value
509 corresponds to a large error, which significantly contributes to a poor NSE value.
510 Therefore, improvements in model accuracy for the peak value simulation of the
511 sediment transport rate require more research.

512 **Table 1. Monthly simulation results of discharge and sediment transport rate at the**
513 **Wenjiachuan hydrological station.**

Items	Indicator	Calibration Period	Verification Period	Whole Period
		1956–1984	1985–2010	1956–2010
Discharge	R	0.87	0.88	0.87
	NSE	0.72	0.78	0.75
	RE (%)	-5.42	4.76	-2.24
Sediment transport rate	R	0.74	0.86	0.76
	NSE	0.54	0.75	0.58
	RE (%)	-8.10	1.80	-5.60

514 ## 5.2. Effects from discharge simulation

The simulated average annual sediment yield is close to the observations throughout the 55 years, only with a relative error of -5.60%. However, the simulation results are affected significantly by the discharge. To further investigate the performance of WEP-SED during high- and low-flow years, we divided these years into two groups, with the average annual discharges from 1956 to 2010, as shown in **Fig.s 15** and **16**. The high-flow group consists of 22 years including 1958, 1959, 1961, 1962, 1964, 1966–1971, 1973, 1976–1979, 1984, 1985, 1988, 1992, 1994, and 1996.

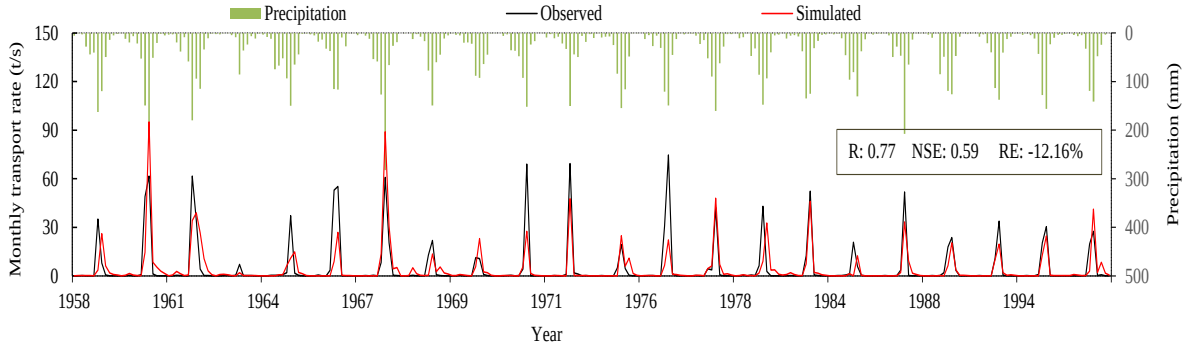

Fig. 15. The observed and simulated monthly sediment transport rate in the high-flow group at the Wenjiachuan hydrological station.

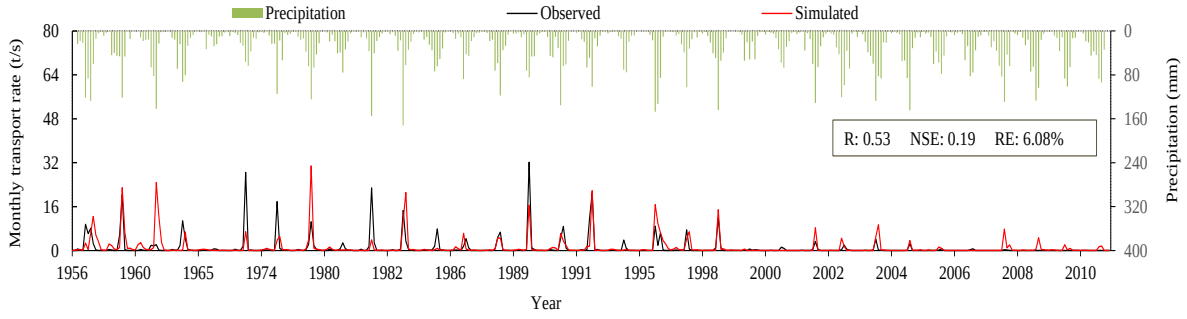

Fig. 16. The observed and simulated monthly sediment transport rate in the low-flow group at the Wenjiachuan hydrological station.

The model performs differently in the high- and low-flow cases. It underestimates the sediment yield during high-flow years but overestimates that

during low-flow years with relative errors of approximate -12% and 6%, respectively. However, the calibrated model performs worse during low-flow years, with only 0.53 and 0.19 for R and NSE respectively in terms of sediment transport rate, than high-flow years. This is mainly a continuation of the large error in discharge simulations during the low-flow years as listed in **Table 2**.

Table 2 Group simulation results of monthly discharge and sediment transport rate from 1956 to 2010 at Wenjiachuan hydrological station

Items	Number of years	Discharge			Sediment transport rate		
		R	NSE	RE (%)	R	NSE	RE (%)
Whole period	55	0.87	0.75	-2.24	0.76	0.58	-5.60
High-flow group	22	0.89	0.79	-6.35	0.77	0.59	-12.16
Low-flow group	33	0.68	0.32	-1.00%	0.53	0.19	6.08

5.3. Model improvements in applicability

The uncertainty in the performance of the WEP-SED is the result of many factors. Several limitations in the model structure and input data are the most relevant.

(i) The sediment transport process in a slope-gully is simplified, with soil erosion estimated directly by transport capacity. In gullied rolling loess regions, the loose soil particles on the slope and in the slope-gully can easily be carried away by runoff. Therefore, soil erosion is usually limited by sediment transport capacity, which is mainly determined by hydrodynamic conditions (Gong et al.,

2011). However, if this model is applied in regions out of the Loess Plateau, the performance of sediment transport equation (20) should be investigated.

(ii) Although the results of the gravitational erosion in this study are reliable for the Loess Plateau, considering only collapses as gravitational erosion may limit the applicability of the WEP-SED in the watersheds where collapses do not dominate gravitational erosion. The gravitational erosion in the form of landslides can be simulated as Wang et al. (2007).

(iii) Human activities have a large influence on the runoff and soil erosion on the Loess Plateau. A significant reduction of both flow discharge and sediment transport rate without a decrease in precipitation can be found in **Figs. 8** and **9**. This is the effect of soil and water conservation measures. However, these measures, such as terraces and check dams, are difficult to simulate accurately because of the lack of data. Multi-source data combined with remote sensing data will be helpful for the applicability of WEP-SED.

6. Conclusions

This study develops a three-process-based distributed soil erosion model based on the WEP-L. The newly developed soil erosion model refines traditional two-process models for the Loess Plateau in China, resulting in an innovative approach to separating gully erosion process from traditional river erosion process. The physically-based gully erosion process, a unique erosion feature on the Loess Plateau, clearly explains the link between slope soil erosion and river

sediment transport. In particular, this research advances our understanding of gravitational erosion based on mechanical equilibrium principle, which yields a more accurate and applicable model. We applied the WEP-SED to analyze soil erosion in the Kuye River basin. The simulated monthly sediment transport rate from 1956 to 2010 at the Wenjiachuan hydrological station is similar to observations with a correlation coefficient of 0.76, an NSE of 0.58, and a relative error of -5.60%, which demonstrates the efficiency and accuracy of the WEP-SED. The calculated average annual quantity of gully erosion is larger than that of slope and river erosion, which reflects the fact that the former is a serious problem in the gullied rolling loess regions of the Loess Plateau and that the gully erosion process is essential to simulating soil erosion in this area. An analysis of the sediment transport rate influenced by the flow discharge indicates that the physical processes associated with runoff and soil erosion are tightly coupled with each other.

This study is a preliminary attempt to perform physically-based simulations of soil erosion in the overall processes and this subject requires further research. Insufficient standard data, including observed gully and gravitational erosion, limit the applicability of the WEP-SED. Further improvements should concentrate on enhancing data quality for model implementation and testing. Moreover, both terraces and check dams are important due to their effects on sediment retention and reduction in erosion. The effects of soil and water conservation, as well as spatial and temporal variation in underlying surfaces,

will be further investigated to improve the mechanisms involved in the three-process-based soil erosion model on the Loess Plateau.

Acknowledgments

This work was supported by the National Key Research and Development Program of China (2016YFC0402405). The reviewers and editors are acknowledged for their comments, which significantly improved the quality of the manuscript.

References

Aksoy, H., Kavvas, M.L., 2005. A review of hillslope and watershed scale erosion and sediment transport models. Catena 64(2-3), 247-271.

Beven, K., 1989. Changing ideas in hydrology-the case of physically-based models. Journal of hydrology 105(1-2), 157-172.

Cai, Q., Lu, Z., Wang, G., 1996. Process-based soil erosion and sediment yield model in a small basin in the hilly loess region. Acta Geographica Sinica 51(2), 108-117.

De Roo, A.P.J., Wesseling, C.G., Ritsema, C.J., 1996. LISEM: a single event physically-based hydrologic and soil erosion model for drainage basins. I: theory, input and output. Hydrol. Process. 10 (8), 1107-1117.

612 Dutta, S., Sen, D., 2018. Application of SWAT model for predicting soil erosion
613 and sediment yield. Sustainable Water Resources Management 4(3), 447-468.
614 Fang X., Wan Z., Kuang, S., 1998. Mechanism and effect of silt-arrest dams for
615 sediment reduction in the middle Yellow River basin. Journal of Hydraulic
616 Engineering 29(10), 49-53.
617 Fu, B., Gulinck, H., 1994. Land evaluation in an area of severe erosion: the
618 Loess Plateau of China. Land Degradation & Development 5(1), 33-40.
619 Gong, J., Jia, Y., Zhou, Z., Wang, Y., Wang, W., Peng, H., 2011. An experimental
620 study on dynamic processes of ephemeral gully erosion in loess landscapes.
621 Geomorphology 125(1), 203-213.
622 Guo, W., 2018. Mechanism and effect of silt-arrest dams for sediment reduction
623 in the middle Yellow River basin. Thesis, Dalian University of Technology.
624 Hajigholizadeh, M., Melesse, A., Fuentes, H., 2018. Erosion and sediment
625 transport modelling in shallow waters: A review on approaches, models and
626 applications. International journal of environmental research and public health
627 15(3), 518.
628 He, X., Zhang, G., Liu, B., 2003. Soil detachment by shallow flow on slopes.
629 Transactions of the CSAE 19(6), 52-55.
630 Hessel, R., Van Asch, T., 2003. Modelling gully erosion for a small catchment
631 on the Chinese Loess Plateau. Catena 54, 131-146.
632 Jakeman, A.J., Hornberger, G.M., 1993. How much complexity is warranted in a
633 rainfall-runoff model? Water Resources Research 29 (8), 2637-2649.

634 Jia, Y., Tamai, N., 1998. Integrated analysis of water and heat balance in Tokyo
635 metropolis with a distributed model. J. Japan Soc. Hydrol. Water Resour. 11
636 (1), 150-163.
637 Jia, Y., Wang, H., Wang, J., Qin, D., 2004. Distributed hydrologic modeling and
638 river flow forecast for water allocation in a large-scale inland basin of
639 Northwest China. In: Proceedings of 2nd APHW Conference, Singapore, 2,
640 285-292.
641 Jia, Y., Wang, H., Zhou, Z., Qiu, Y., Luo, X., Wang, J., Yan, D., Qin, D., 2006.
642 Development of the WEP-L distributed hydrological model and dynamic
643 assessment of water resources in the Yellow River basin. Journal of
644 Hydrology 331(3-4), 606-629.
645 Jiang, Z., Song, W., Li, X., 1983. Study on the Characteristics of Natural
646 Raindrop in loess areas. Soil and Water Conservation in China 3(18), 32-36.
647 Jing K., 1986. A study on gully erosion on the Loess Plateau. Scientia
648 Geographica Sinica 6(4), 340-347.
649 Kandel, D.D., Western, A.W., Grayson, R.B., Turral, H.N., 2004. Process
650 parameterization and temporal scaling in surface runoff and erosion modelling.
651 Hydrological Processes 18(8), 1423-1446.
652 Kim, H., Noh, S., Jang, C., Kim, D., Hong, I., 2005. Monitoring and analysis of
653 hydrological cycle of the Cheonggyecheon watershed in Seoul, Korea. In
654 Proceedings of International Conference on Simulation and Modeling,
655 Nakornpathom, Thailand, pp. 17-19.

656 Laflen, J.M., Lane, L.J., Foster, G.R., 1991. WEPP: A new generation of erosion
657 prediction technology. Journal of Soil and Water Conservation 46, 34–38.
658 Li, C., Qi, J., Feng, Z., Yin, R., Guo, B., Zhang, F., Zou, S., 2010. Quantifying
659 the effect of ecological restoration on soil erosion in China's Loess Plateau
660 region: an application of the MMF approach. Environmental Management
661 45(3), 476-487.
662 Li, P., Mu, X., Holden, J., Wu, Y., Irvine, B., Wang, F., Gao, P., Zhao, G., Sun,
663 W., 2017. Comparison of soil erosion models used to study the Chinese Loess
664 Plateau. Earth-Science Reviews 170, 17-30.
665 Li, Z., Liu, W., Zhang, X., Zheng, F., 2011. Assessing the site-specific impacts
666 of climate change on hydrology, soil erosion and crop yields in the Loess
667 Plateau of China. Climatic Change 105(1-2), 223-242.
668 Merritt, W.S., Letcher, R.A., Jakeman, A.J., 2003. A review of erosion and
669 sediment transport models. Environmental Modelling & Software 18(8-9),
670 761-799.
671 Morgan, R.P., Quinton, J.N., 2001. Erosion modeling. In Landscape erosion and
672 evolution modeling (pp. 117-143). Springer, Boston, MA.
673 Morgan, R.P.C., Quinton, J.N., Smith, R.E., Govers, G., Poesen, J.W.A.,
674 Auerswald, K., Chisci, G., Torri, D., Styczen, M.E., 1998. The European Soil
675 Erosion Model (EUROSEM): a dynamic approach for predicting sediment
676 transport from fields and small catchments. Earth Surface Processes and

677 Landforms: The Journal of the British Geomorphological Group 23(6),
678 527-544.
679 Nash, J.E., Sutcliffe, J.V., 1970. River flow forecasting through conceptual
680 models - Part I: A discussion of principles. Journal of hydrology 10(3),
681 282-290.
682 NSERL, 1995. WEPP User Summary Version 95.7, National Soil Erosion
683 Research Laboratory Report No. 11.
684 Pandey, A., Himanshu, S.K., Mishra, S.K., Singh, V.P., 2016. Physically based
685 soil erosion and sediment yield models revisited. Catena 147, 595-620.
686 Poesen, J., 2018. Soil erosion in the Anthropocene: Research needs. Earth
687 Surface Processes and Landforms 43(1), 64-84.
688 Prosser, I.P., Rustomji, P., 2000. Sediment transport capacity relations for
689 overland flow. Progress in Physical Geography 24(2), 179-193.
690 Qiu, Y., Wang, S., Jia, Y., Wang, H. 2006. Preliminary analysis of hydrological
691 and water resources effects under the impacts of water and soil conservation
692 engineering in the Fenhe river basin. Journal of Natural Resources 21(1),
693 24-30.
694 Renard, K.G., Foster, G.R., Weesies, G.A., McCool, D.K., Yoder, D.C., 1997.
695 Predicting soil erosion by water: a guide to conservation planning with the
696 Revised Universal Soil Loss Equation (RUSLE) (Vol. 703). Washington, DC:
697 United States Department of Agricultur.

Sadeghi, S.H.R., Gholami, L., Khaledi Darvishan, A., Saeidi, P., 2014. A review of the application of the MUSLE model worldwide. Hydrological Sciences Journal 59(2), 365-375.

Si, W., Bao, W., Jiang, P., Zhao, L., Qu, S., 2017. A semi-physical sediment yield model for estimation of suspended sediment in loess region. International Journal of Sediment Research 32(1), 12-19.

Sorooshian, S., 1991. Parameter estimation, model identification, and model validation: Conceptual-type models. In Recent Advances in the Modeling of Hydrologic Systems; Springer: Berlin/Heidelberg, Germany, pp. 443-467.

Tang, L., Chen, G., 1997. A Dynamic Model of Runoff and Sediment Yield from Small Watershed. Journal of Hydrodynamics 12(2), 164-174.

Wainwright, J., Mulligan, M. (Eds.), 200 Environmental modelling: finding simplicity in complexity. John Wiley & Sons.

Wang, G., Wu, B., Li, T., 2007. Digital yellow river model. Journal of Hydro-Environment Research 1(1), 1-11.

Wang, G., Xue, H., Li, T., 2005. Mechanical model for gravity erosion in gully area. Journal of Basic Science and Engineering 13(4), 335-344.

Williams, J.R., Renard, K.G., Dyke, P.T., 1983. EPIC: A new method for assessing erosion's effect on soil productivity. Journal of Soil and water Conservation 38(5), 381-383.

718 Wischmeier, W. H., Smith, D.D., 1978. Predicting Rainfall Erosion Losses - a
719 guide to conservation planning. Agricultural Research Service Handbook 537.
720 United States Department of Agriculture, Washington, D.C.
721 Wu, P., Zhou, P., 1992. The action of raindrop splash on sheet flow erosion.
722 Bulletin of soil and water conservation 12(4):19-26, 47.
723 Xu, J.X., 1999. Erosion caused by hyperconcentrated flow on the Loess Plateau
724 of China. Catena 36(1-2), 1-19.
725 Xue, Y.W., Lin, L.Z., 2000. Reliability Analysis of Maximum Observed
726 Sediment Concentration at Wenjiachuan Station. Journal of China Hydrology
727 20(3), 41-43.
728 Zhang, H., 1992. Formula of Sediment Carrying Capacity of the Yellow River.
729 Yellow River (11), 7-9.
730 Zhang, X., Li, Z., Ding, W., 2005. Validation of WEPP sediment feedback
731 relationships using spatially distributed rill erosion data. Soil Science Society
732 of America Journal 69(5), 1440-1447.
733 Zhang, X., Liu, W., 2005. Simulating potential response of hydrology, soil
734 erosion, and crop productivity to climate change in Changwu tableland region
735 on the Loess Plateau of China. Agricultural and Forest Meteorology 131(3-4),
736 127-142.
737 Zuo, D., Xu, Z., Yao, W., Jin, S., Xiao, P., Ran, D., 2016. Assessing the effects of
738 changes in land use and climate on runoff and sediment yields from a

watershed in the Loess Plateau of China. Science of the Total Environment 544, 238-250.